Activities, Crystal Structures, and Molecular Dynamics of Dihydro-1*H*-isoindole Derivatives, Inhibitors of HIV-1 Integrase

Mathieu Métifiot,[†,⊥] Kasthuraiah Maddali,[†,⊥] Barry C. Johnson,[§] Stephen Hare,[‡] Steven J. Smith,[§] Xue Zhi Zhao,[∥] Christophe Marchand,[†] Terrence R. Burke, Jr.,[∥] Stephen H. Hughes,[§] Peter Cherepanov,[‡,#] and Yves Pommier*,[†]

[†]Laboratory of Molecular Pharmacology, Center for Cancer Research, National Cancer Institute, National Institutes of Health, 37 Convent Drive, Bethesda, Maryland 20892, United States
[‡]Division of Infectious Diseases, Imperial College London, London, U.K.
[§]HIV Drug Resistance Program and [∥]Chemical Biology Laboratory, Molecular Discovery Program, Center for Cancer Research, Frederick National Laboratory, National Institutes of Health, Frederick, Maryland 21702, United States
[#]Cancer Research UK London Research Institute, Clare Hall Laboratories, Potters Bar, Hertfordshire, UK

ⓢ *Supporting Information*

ABSTRACT: On the basis of a series of lactam and phthalimide derivatives that inhibit HIV-1 integrase, we developed a new molecule, XZ-259, with biochemical and antiviral activities comparable to raltegravir. We determined the crystal structures of XZ-259 and four other derivatives in complex with the prototype foamy virus intasome. The compounds bind at the integrase-Mg^{2+}-DNA interface of the integrase active site. In biochemical and antiviral assays, XZ-259 inhibits raltegravir-resistant HIV-1 integrases harboring the Y143R mutation. Molecular modeling is also presented suggesting that XZ-259 can bind in the HIV-1 intasome with its dimethyl sulfonamide group adopting two opposite orientations. Molecular dynamics analyses of the HIV-1 intasome highlight the importance of the viral DNA in drug potency.

Binding of XZ-259 within the PFV intasome
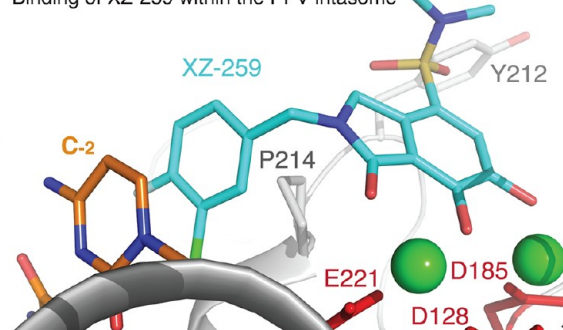
After 30 years of research, the clinical armamentarium available for the treatment of HIV infections has grown to about 30 drugs. The classical anti-HIV drugs target reverse transcriptase (RT) and protease (PR). With the remarkable clinical activity of raltegravir (RAL, Merck), HIV integrase (IN) has become an invaluable therapeutic target. Integration of the viral DNA into the cellular genome is required for viral replication [for a review, see refs 1 and 2]. Integration involves two distinct steps, both of which are catalyzed by IN. Following reverse transcription in the cytoplasm, IN cleaves two nucleotides from both 3′-ends of the viral DNA in the preintegration complex (PIC). Following this 3′-processing (3′-P) reaction, the PIC translocates to the nucleus, where IN catalyzes the joining of the 3′ ends of the viral DNA to chromosomal DNA in the strand transfer (ST) reaction.

RAL was approved by the U.S. Food and Drug Administration (FDA) in 2007 as the first IN inhibitor to treat HIV/AIDS.[3,4] RAL and related IN strand transfer inhibitors (INSTIs) bind to the viral DNA-IN interface in the IN active site.[5−7] Similarly to other anti-HIV drugs, treatment with INSTIs selects for resistant viruses.[8] Clinical resistance to RAL involves three main genetic pathways involving mutations at IN amino acids Y143, Q148, and N155.[8−10] Using a panel of recombinant INs that carry the Y143R, N155H, and G140S-Q148H mutations, we reported that elvitegravir (EVG, Gilead Sciences), dolutegravir (DTG, ViiV Healthcare/Shionogi),

and MK-0536 (Merck) retain high efficacy against these RAL-resistant mutants.[11−14]

Recent structures of the prototype foamy virus (PFV) IN with viral and target DNA substrates have elucidated the architecture of the functional intasome.[6,15] Moreover, cocrystal structures with several INSTIs, including three that are clinically used, RAL, EVG and DTG, demonstrated that these drugs share a common mechanism of action.[6,13,16] They bind to the protein–DNA interface in the IN active site while coordinating the two catalytic magnesium ions bound to the three catalytic amino acids in the enzyme's active site (DDE motif). INSTI binding requires the displacement of the nucleobase of the terminal adenosine (adenosine at position −1, A$_{-1}$) at the 3′ end of the viral DNA and its disengagement from the active conformation.[6,17] This allows the halobenzyl group, present in all INSTIs, to stack with the penultimate cytosine at the 3′ end of the viral DNA (cytosine at position −2, C$_{-2}$). Thus, INSTIs act as interfacial inhibitors.[1,5]

We previously described a series of novel dihydroxy-1*H*-isoindole-based compounds generated by efficient synthetic pathways.[18,19] These derivatives, including XZ-89, XZ-90, XZ-115,

Table 1. Summary of the Biochemical and Cellular Data[a]

XZ-89 · XZ-115 · XZ-116 · XZ-90 · XZ-259 · RAL

		XZ-89 $IC_{50} \pm SD$	FR	XZ-115 $IC_{50} \pm SD$	FR	XZ-116 $IC_{50} \pm SD$	FR	XZ-90 $IC_{50} \pm SD$	FR	XZ-259 $IC_{50} \pm SD$	FR	RAL $IC_{50} \pm SD$	FR
ST	WT	0.5 ± 0.1		0.9 ± 0.2		2.2 ± 0.3		1.1 ± 0.2		0.077 ± 0.004		0.071 ± 0.004	
	Y143R	1.1 ± 0.2	2.2	1.6 ± 0.1	1.8	6.6 ± 0.3	3.0	2.5 ± 0.3	2.3	0.20 ± 0.02	2.5	2.6 ± 0.2	37
	N155H	1.7 ± 0.3	3.4	3.1 ± 0.3	3.4	6.2 ± 0.6	2.8	4.0 ± 0.5	3.6	0.30 ± 0.03	3.9	0.72 ± 0.05	10
	SH	8.5 ± 1.0	17	8.0 ± 1.0	8.9	88.5 ± 5.0	40	55.0 ± 7.0	50	4.4 ± 0.4	57	10.7 ± 0.9	150
3'-P	WT	24.2 ± 2.8		29.0 ± 4.3		158.0 ± 22.3		83.9 ± 6.8		8.6 ± 0.6		30.3 ± 8.5	
Antiviral	WT	1.7 ± 0.5		0.7 ± 0.1		0.5 ± 0.04		0.45 ± 0.11		0.011 ± 0.003		0.004 ± 0.002	
	Y143R	1.8 ± 0.2	1.1	1.2 ± 0.2 *	1.8	0.6 ± 0.2	1.2	0.37 ± 0.08	0.8	0.020 ± 0.006	1.8	0.21 ± 0.01	53
	N155H	5.0 ± 1.0 *	2.9	6.8 ± 1.3 *	10	1.2 ± 0.1	2.3	1.1 ± 0.2	2.5	0.5 ± 0.1	46	0.15 ± 0.03	39
	SH	7.8 ± 1.6 *	4.6	8.4 ± 1.9 *	13	4.4 ± 1.3	8.5	3.6 ± 0.7	8.0	6.8 ± 0.8 *	642	1.7 ± 0.01	425
Toxicity		5.4 ± 1.3		5.1 ± 0.6		7.8 ± 2.1		5.2 ± 0.2		6.6 ± 0.4		>100	

[a]Values are expressed in μM as the mean of at least three independent determinations ± standard deviation (SD). Fold-resistance (FR) corresponds to the ratio of IC_{50} for a particular mutant over WT. SH stands for IN mutation G140S-Q148H. [b]EC_{50} values in the range of the CC_{50} value.

and XZ-116 (Table 1), have common characteristic features with established INSTIs: a halogen-substituted ring linked to a chelating core consisting in a combination of three oxygen or nitrogen atoms.[20] Herein, we report a new derivative, XZ-259, with improved inhibitory potencies in biochemical and antiviral assays against WT and RAL-resistant integrases. Its cocrystal structure has been solved along those of the four other derivatives in the PFV intasome. Molecular dynamics simulations were performed using an HIV-1 IN homology model derived from these PFV intasome crystal structures.

■ RESULTS AND DISCUSSION

Inhibition of Recombinant WT IN. We initiated our study with four structurally related compounds, XZ-89, XZ-90, XZ-115, and XZ-116 (Table 1), that inhibit IN with IC_{50} values in the low- to submicromolar range for the ST reaction and in the high micromolar range for the 3′-P reaction.[18,19] Although these early derivatives are relatively weak HIV-1 IN inhibitors, XZ-89 and XZ-90 have slightly lower IC_{50} values for ST than XZ-115 and XZ-116 (around 2-fold, Table 1), which can be attributed, at least in part, to their halogen substitution pattern. While the four compounds contain a *meta*-chlorine, the fluoro substituent is *para* for XZ-89 and XZ-90 and *ortho* for XZ-115 and XZ-116 (Table 1). Additionally, the addition of a carbonyl group in XZ-89 and XZ-115 resulted in an approximate 2-fold increase in ST inhibition potency compared to XZ-90 and XZ-116.

Because the introduction of a carbonyl on the isoindoline ring system appeared to be beneficial, we explored the effect of a larger substitution. XZ-259 was derived from XZ-90 by the addition of a dimethyl sulfonamide to the 4-position of the 1-oxoisoindoline ring (Table 1). This new compound was markedly more potent with an IC_{50} value of 77 nM against ST, similar to that of RAL (Figure 1A,B). Additionally, XZ-259 was more potent than RAL at inhibiting 3′-P (Table 1). These results demonstrate that the introduction of a 5-membered ring scaffold is compatible with potent IN inhibition.

Inhibition of RAL-Resistant Enzymes in Biochemical Assays. The dihydro-1*H*-isoindole derivatives were tested against a panel of recombinant INs carrying mutations Y143R,
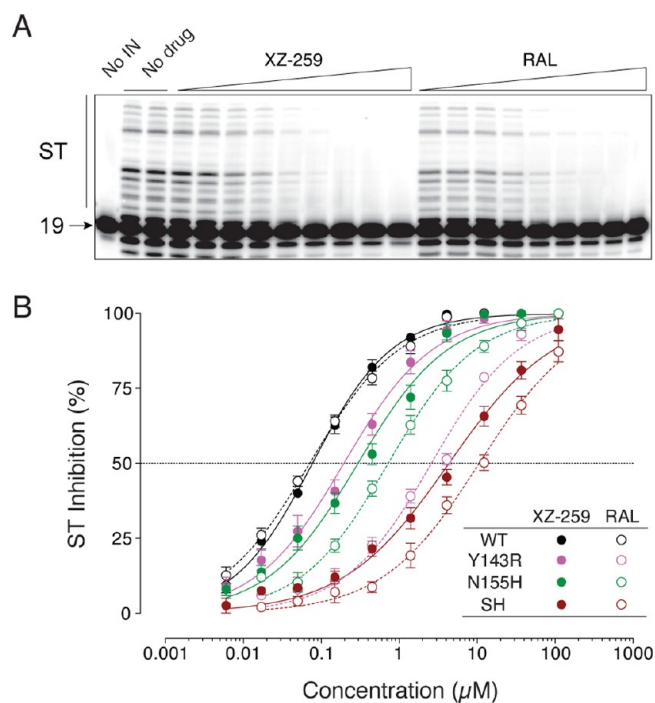

Figure 1. IN inhibitory activity of XZ-259 compared to RAL. (A) Representative gel showing ST inhibition of WT IN by XZ-259 and RAL (serial dilutions from 17 nM to 111 μM following a 3-fold increment). (B) Differential inhibition of WT and RAL-resistant INs by XZ-259 and RAL. ST inhibition was monitored using gel-based assays. Means and standard deviations (SD) derived from at least 3 independent experiments.

N155H, or G140S-Q148H that are known to cause RAL-resistance.[7,11,12] RAL's oxadiazole substituent is known to interact with Y143 through π-stacking.[6] Therefore, our compounds that lack this substituent should retain potency against IN harboring mutation at residue Y143.[12] As expected, the Y143R mutation had minimal impact on the activity of our five derivatives (less than
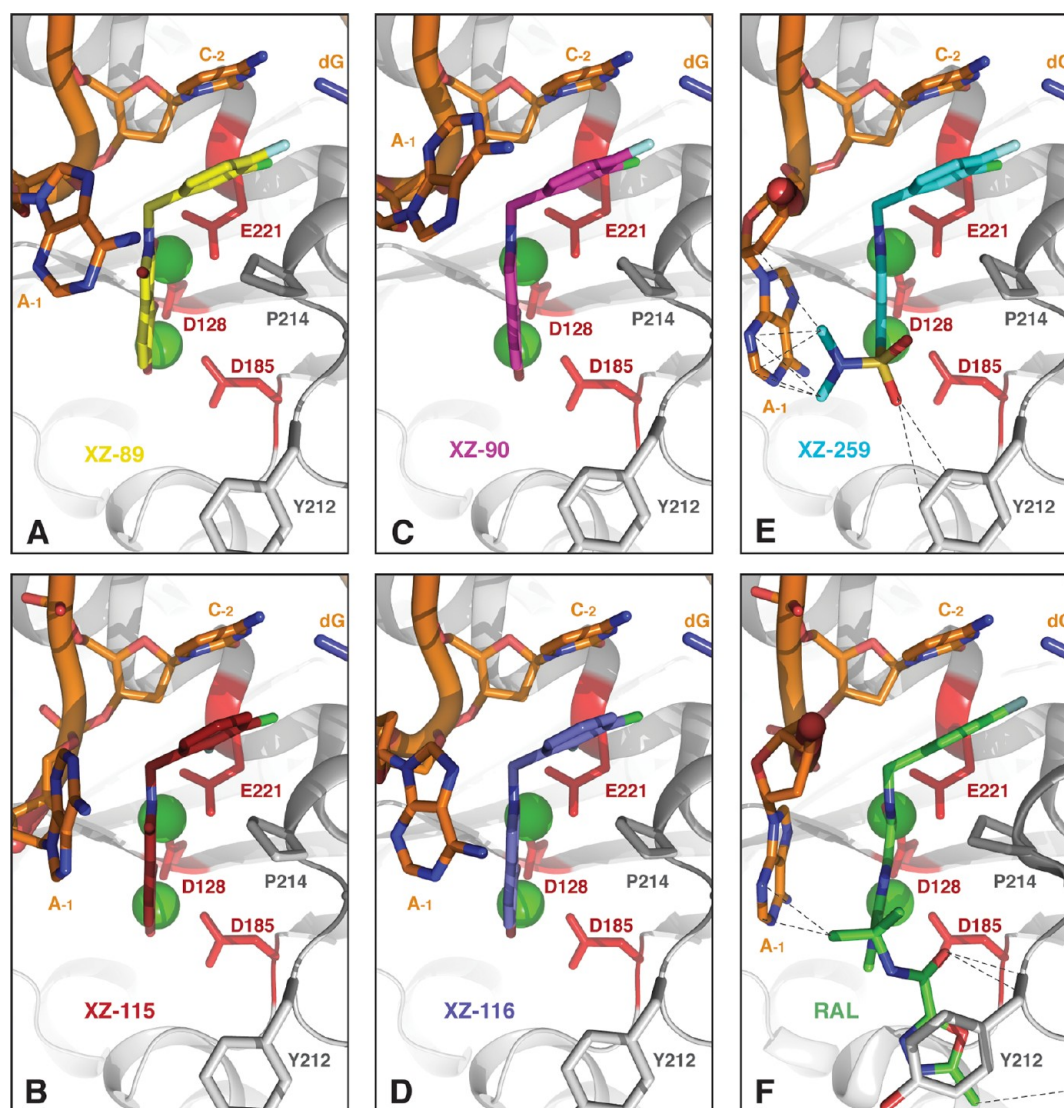
Figure 2. Co-crystal structures of the INSTIs in the PFV intasome. IN and its viral DNA substrate are represented in gray and orange, respectively. Residues D128, D185, E221, Y212, and P214 (corresponding to D64, D116, E152, Y143, and P145 in HIV-1) are shown in red and gray sticks, respectively. The two Mg^{2+} ions are represented as green spheres. The terminal viral dinucleotide CA is shown as sticks and colored by elements (N, blue; O, red; C, orange). The drugs (XZ-89, panel A; XZ-115, panel B; XZ-116, panel D; XZ-90, panel C; XZ-259, panel E; RAL, panel F) are represented as yellow, red, dark blue, magenta, cyan, or green sticks and colored by element (N, blue; O, red; F, light blue; Cl, green). Potential VdW contacts (<4 Å) are represented by dashed lines.

3-fold), whereas it induced a loss of sensitivity to RAL (37-fold increase in IC_{50}) (Figure 1B).

The entire series showed only a modest susceptibility to the N155H mutation, with a 3- to 4-fold increase in ST IC_{50} values compared to WT (Table 1). In contrast, the N155H mutation causes a 10-fold reduction in susceptibility to RAL.[11] Thus, in the biochemical assays with recombinant IN, XZ-259 is more potent than RAL against the N155H mutant, with an IC_{50} value of 300 nM versus 720 nM, respectively (Table 1 and Figure 1B).

The double mutation G140S-Q148H resulted in high resistance to XZ-90 and XZ-116 (up to 50-fold increase in ST IC_{50}, Table 1). However, we observed lower fold-changes in IC_{50} value with XZ-115 and XZ-89 (9- to 17-fold). Although the halogen substitution pattern influenced the overall inhibitory potency of the series (*para* > *ortho*, see previous section), the presence of an additional keto-group on the isoindole skeleton, as seen in XZ-89 and XZ-115, affected the resistance profile. This might be because the carbonyl either allows additional interaction

within the active site or affects the electronic properties of the metal binding oxygens, thus improving the metal chelation (see below).

The G140S-Q148H mutant induced resistance to the new derivative XZ-259 with a 57-fold increase in IC_{50} (Table 1). Nevertheless, XZ-259 remained the most active compound with an IC_{50} nearly 3-fold lower than that of RAL (which exhibited a 150-fold increase in IC_{50} value). Thus, the introduction of a dimethyl sulfonamide greatly improved the potency of the compounds against the WT enzyme but only partially increased the potency against the G140S-Q148H double mutant.

Together, these biochemical experiments show that XZ-259 is comparable to RAL against WT IN. It retains potency against the RAL-resistant Y143R mutant and partial efficacy against the N155H mutant. Yet, XZ-259 inhibits the N155H mutant less potently than DTG or MK-0536.[13,14]

Antiviral Activity. The antiviral activity of the five XZ derivatives was measured in cell-based assays using a single-round

HIV vector[18] in parallel with RAL. In this assay, XZ-89 was antiviral at low micromolar concentrations with an EC_{50} value of 1.7 μM; more than three times the concentration needed to achieve 50% inhibition of ST catalyzed by recombinant IN (Table 1). The other compounds were more potent, with EC_{50} values ranging from 700 nM for XZ-115 to 11 nM for XZ-259 (Table 1). While RAL and XZ-259 had the same IC_{50} in our biochemical assays, the EC_{50} for RAL was 3-fold lower than that of XZ-259 in the antiviral assay. The antiviral activity of XZ-259 was, however, comparable to that of RAL with a low nanomolar EC_{50}.

XZ-89, XZ-90, XZ-115, XZ-116, and XZ-259 showed cytotoxicity at low micromolar concentrations (Table 1). In the same experiments, RAL was nontoxic up to the maximal concentration tested (100 μM). Because they are cytotoxic, it appears that our derivatives enter cells efficiently but have additional cellular target(s). Further modification of this simple chemotype is likely to reduce this off-target effect. Nevertheless, XZ-259 represents a step forward in the series because of their improved therapeutic index [CC_{50}/EC_{50} of 660 as compared to 5–20 for the earlier compounds (Table 1)].[18,19]

Consistent with our biochemical assays, the Y143R mutation had minimal effect on the antiviral potency of our dihydro-1H-isoindole series (including XZ-259) with less than 2-fold increase in EC_{50} values. Under the same conditions, RAL lost considerable potency (53-fold increase in EC_{50} value, Table 1). Consequently, XZ-259 is over 10 times more potent than RAL at inhibiting the Y143R mutant virus.

In the context of the N155H and G140S-Q148H mutants, several EC_{50} values were in the range of the CC_{50} (e.g., for XZ-89 and XZ-115). In those cases, the inhibition observed is probably a combination of cytotoxicity and antiviral activity.

The N155H mutant was similarly susceptible as the WT virus to inhibition by XZ-90 and XZ-116 (less than 3-fold increase in EC_{50}). Yet, this mutation caused a similar loss of activity for RAL and XZ-259 (39- and 46-fold increase in EC_{50}, respectively). Thus, XZ-259 is 3-time less potent than RAL against the N155H mutant virus but still remains at least 2 times more potent than our previous compounds (Table 1).

As expected from our biochemical data, the G140S-Q148H mutant caused a large increase in the EC_{50} values for RAL and XZ-259 to 1.7 and 6.8 μM, respectively (Table 1). The four initial compounds, XZ-90 and XZ-116 were less susceptible to this double mutation (Table 1). However, these derivatives are weak antiviral inhibitors and, in the context of the G140S-Q148H mutant, are at least 2-fold less potent than RAL.

Taken together, these results show that XZ-259 has comparable antiviral activity to RAL against the WT virus. It also overcomes the Y143R mutation but not the N155H and G140S-Q148H mutations.

Structural Studies with the PFV Intasome. Because of the high amino-acid sequence identity within active sites of retroviral integrases, the PFV intasome provides an invaluable system for analyzing the binding of INSTIs.[6,13,16] The structures can then serve for homology modeling of HIV-1 complexes.[22,23] Cocrystal structures for our five derivatives showed that the compounds share with RAL a common binding mode to the intasome (Figure 2). The introduction of a sulfonamide group as in XZ-259 enables van der Waals (VdW) interactions with Y212 (corresponding to residue Y143 of HIV-1). While the π-stacking occurring in the case of RAL requires a tyrosine residue, these VdW interactions do not. Because the Y143R mutant has only a minimal effect on the activity of XZ-259, it seems that the

additional interactions enabled with the dimethyl sulfonamide are conserved in this arginine mutant. Moreover, the dimethyl sulfonamide group enables VdW interactions with the sugar and base of the terminal adenine base (A$_{-1}$, Figure 2E). Taken together, these additional interactions probably account for the increased potency of XZ-259 over our previous derivatives (see below).

Figure 3A shows that the positions of the three oxygen atoms interacting with the catalytic Mg^{2+} ions are conserved among our
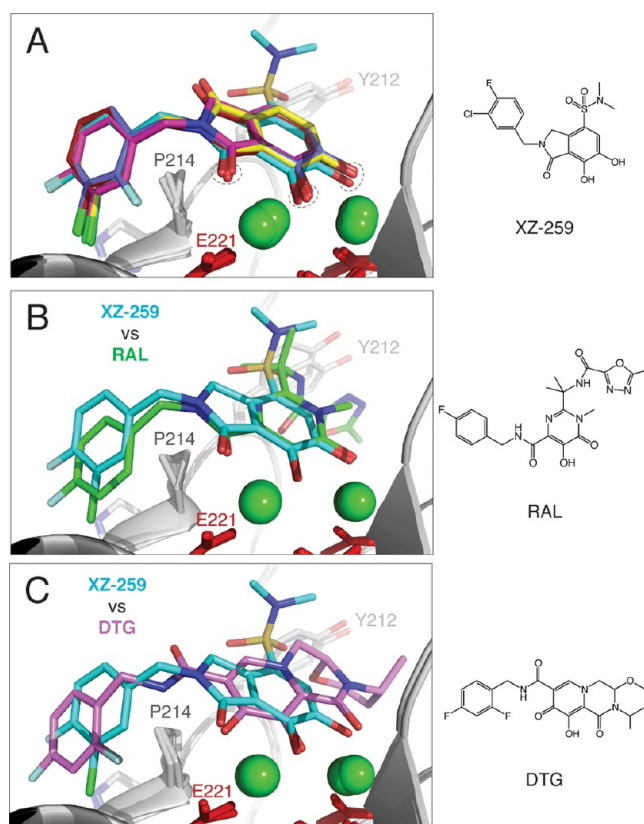

Figure 3. Comparison of the compounds' halobenzyl ring interactions within the PFV intasome. (A) Overlaid structures of the five XZ derivatives. The position of the oxygen atoms in interaction with the metal ions is highlighted with dashed circles. (B,C) Overlaid cocrystal structure of XZ-259 with RAL (B) and DTG (C) (pdb IDs 3OYA, and 3S3M, respectively). IN is represented in gray and residues D128, D185, E221, Y212, and P214 (corresponding to D64, D116, E152, Y143, and P145 in HIV-1) are shown in red and dark gray sticks. The compounds (XZ-89, XZ-115, XZ-116, XZ-90, XZ-259, RAL, and DTG) are represented as yellow, red, purple-blue, magenta, cyan, green, or violet sticks and colored by element (N, blue; O, red; F, light blue; Cl, green). Additionally, the structures of XZ-259, RAL, and DTG are reported next to each panel.

five derivatives (dashed circles). Only minor shifts in metal coordination geometry were observed (less than 0.9 Å) and were within variation observed with other INSTIs (Figure 3B,C).[16] Therefore, the introduction of a 5-membered ring in our compounds compared to RAL does not significantly perturb the interactions of the compounds with the Mg^{2+} ions.

Figures 2 and 3 show that the halobenzyl ring of our five derivatives bind to the same IN-DNA hydrophobic pocket as RAL, created between residues P214, Q215, and E221 (P145, Q146, and E152 in HIV-1 IN) and the C:G base-pair. Because the halobenzyl rings of XZ-89, XZ-90, XZ-115, and XZ-116
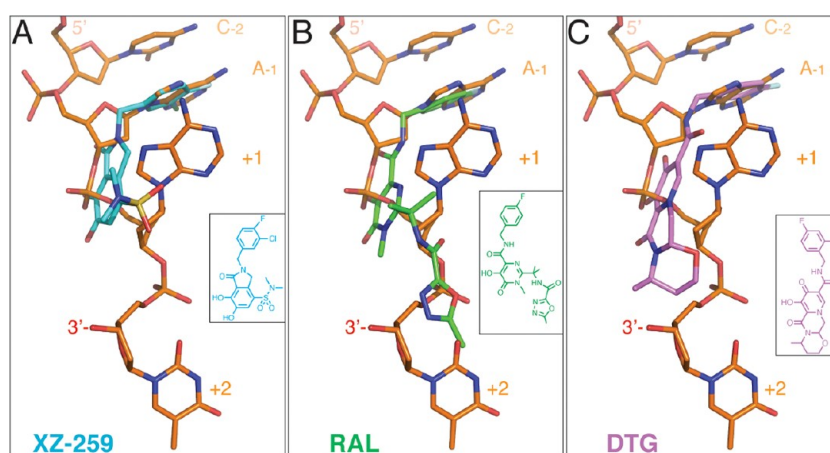
Figure 4. Position of the INSTIs compared the full-length viral DNA in the PFV intasome. Cocrystal structures of XZ-259 (A), RAL (B), and DTG (C) were overlaid with the structure of the PFV intasome before 3'-P (pdb ID 4E7I).[24] The insets show the compounds' chemical structure. The terminal CAAT (corresponding to CAGT for HIV-1) and the inhibitors are shown as sticks and colored by elements according to Figure 2. The adenosine and thymidine following the conserved C_{-2} and A_{-1} (corresponding to guanosine and thymidine in HIV-1 viral DNA) are indicated as +1 and +2, respectively.
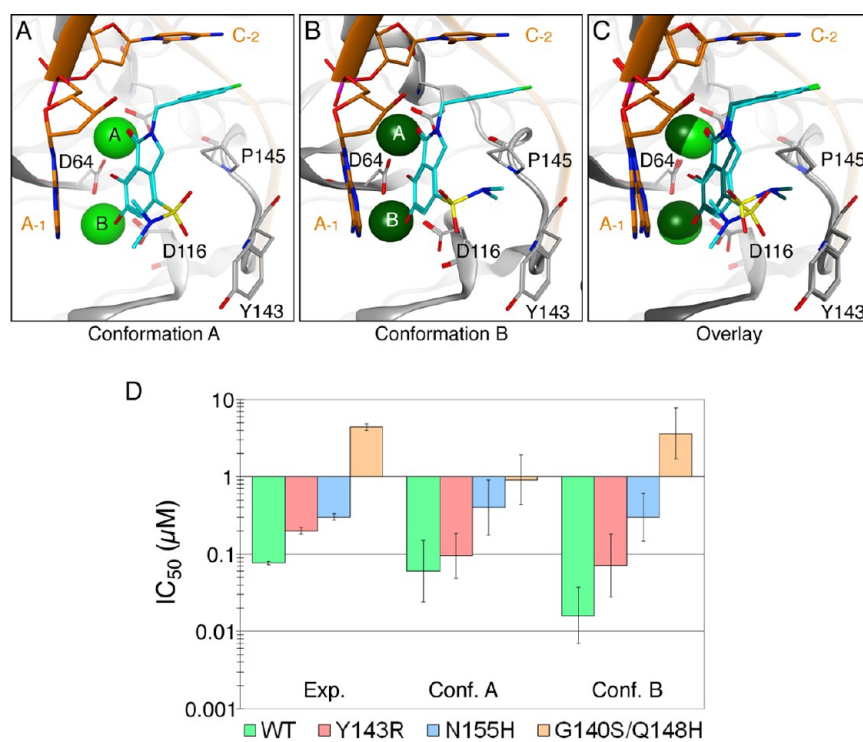

Figure 5. HIV-1 IN homology model with XZ-259. (A–C) IN and its viral DNA substrate are represented as gray and orange cartoons, respectively. Active site residues D64, D116, and E152, as well as flexible loop residues Y143 and P145, are shown as gray sticks. Magnesium ions are represented as green spheres. The terminal C_{-2} and A_{-1} are shown as orange sticks and colored by element (N, blue; O, red; C, orange). XZ-259 is represented as cyan sticks and colored by element (N, blue; O, red; S, yellow; F, light green; Cl, dark green). Panels A and B correspond to XZ-259's A and B conformations, respectively. Panel C shows an overlay of both the A and B conformations of XZ-259. (D) Experimental and predicted IC_{50} values for XZ-259. Experimentally determined values were compared to those predicted by MD analysis for each conformation of XZ-259. WT and mutant INs are color-coded as indicated.

superimpose with that of XZ-259 (Figure 3A), we focused on XZ-259 to compare our derivatives with RAL and DTG. The halobenzyl rings of RAL and DTG lie approximately 1.5 Å deeper than XZ-259 into the hydrophobic pocket [toward E221 (RAL) and the guanosine of the noncleaved DNA strand (DTG)] which could reduce the interaction of the XZ compounds. The difference in position of the halobenzyl

rings may be related to the linker connecting it to the chelating core. The linker of DTG contains flexible bonds (Figure 3C). Our series incorporates the same linker as RAL (−N−), but the nitrogen is part of a 5-membered ring system (Figure 3B), which may increase constraint on the linker, preventing the halobenzyl ring from optimally engaging in the hydrophobic pocket. These results suggest that replacing the single rotatable
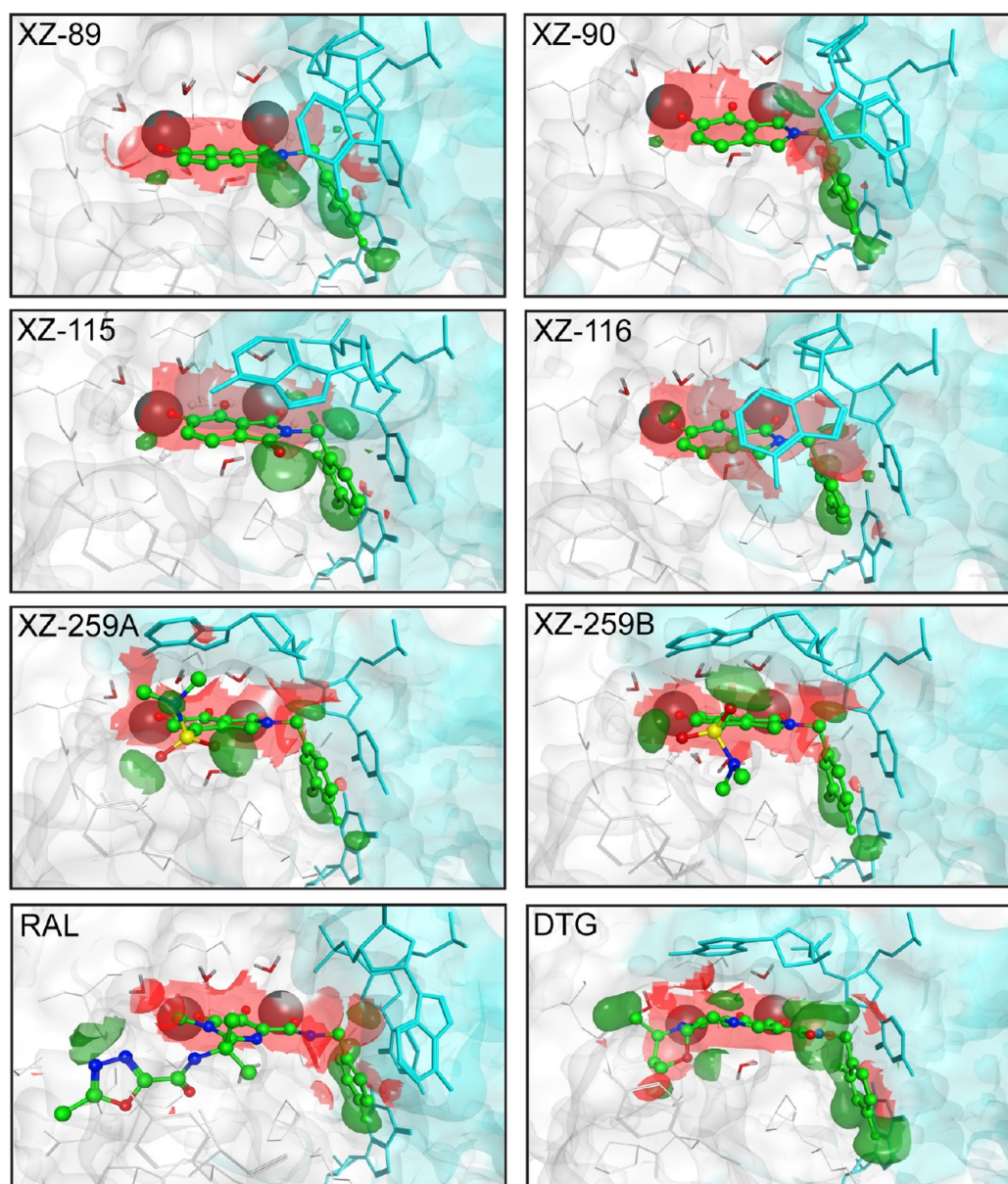
Figure 6. Analysis of solvation effects on INSTI binding. Modeled HIV-1 IN and the viral DNA substrate are shown as white and cyan semitransparent surfaces, respectively. In the PFV intasome structures, the terminal adenosine is poorly resolved probably because its actual position in solution is dynamic or because different conformations are in equilibrium. Here, we placed the base according to the best fit of the electron density data in the PFV intasome structures. INSTIs are shown as ball and stick representations colored by atom type (C, green; N, blue; O, red; S, yellow), magnesium ions are shown as dark gray spheres, and water molecules are shown as sticks. Binding $\Delta G_{solvation}$ was mapped for each XZ compound (including both conformations of XZ-259), as well as RAL and DTG. Green surfaces represent areas where $\Delta G_{solvation} \leq -0.2$ kcal/mol/Å^3, and red surfaces represent areas where $\Delta G_{solvation} \geq 0.2$ kcal/mol/Å^3.

carbon by a longer and more flexible linker (as in DTG) may improve the ability of the ring systems to interact with the IN−DNA complex.[13]

Recently, the structure of the PFV intasome immediately prior to 3′-P has been resolved, including the full-length viral DNA ($C_{-2}A_{-1}A_{+1}T_{+2}$ corresponding to $C_{-2}A_{-1}G_{+1}T_{+2}$ for HIV-1).[24] This structure highlights the complete DNA binding pocket. To assess whether INSTIs take full advantage of this binding pocket, we overlaid this structure onto our cocrystal structures. Figure 4 shows the position of XZ-259, RAL, and DTG relative to the DNA before 3′-P. As previously described,[6] the halobenzyl rings of INSTIs occupy the space of the A_{-1} (i.e., the adenosine of the conserved CA, Figure 4). XZ-259 has limited overlap with the viral DNA past this A_{-1}. Only one oxygen atom of the dimethyl sulfonamide group overlaps the base of the A_{+1} (0.2 Å from the adenine N9, see Figure 4A). However, both RAL and DTG extend toward the sugar of the A_{+1} and the phosphodiester bond between A_{+1} and T_{+2}. Therefore, one possibility for improving XZ-259 would be to extend the molecule to occupy the space corresponding to the +1 nucleotide.

Molecular Modeling of the Compounds into the HIV-1 Intasome. Next, we used our cocrystal structures and homology model for HIV-1 IN [22] to generate models of the new compounds bound to HIV-1 IN. The lowest energy conformation of XZ-259 in the HIV-1 intasome differed from its conformation in the PFV IN cocrystal by the dimethyl sulfonamide orientation (Figure 5B). In the PFV IN structure, the two methyl groups face the A_{-1}, while the two oxygen

atoms point toward P214 (P145 in HIV-1, conformation A, Figure 5A). In the HIV-1 IN model, the dimethyl sulfonamide substituent was flipped 180° with the oxygen atoms facing A$_{-1}$ and the methyl groups against P145 (conformation B, Figure 5B). We modeled conformation A in the HIV homology model, and switching from conformation A to conformation B had only minor effects on the protein side chains and metal ions in the active site (Figure 5C). The magnesium ion closest to the penultimate cytosine (magnesium A) shifted 0.36 Å, while the other magnesium ion (magnesium B) shifted 0.27 Å (Figure 5). There were minor differences in the position of the oxygen atoms of the DDE motif, the drug, and the surrounding water molecules that are involved in metal-binding. The mean shift of oxygens binding magnesium A is 0.28 Å, and that binding magnesium B is 0.25 Å. The plane of the drug's chelating core was tilted between the two conformations, leading to a difference of 0.83 Å in the location of the sulfur atom.

We previously described a MD approach that made it possible to correlate the interaction energy of the magnesium ions with the *in vitro* IC$_{50}$ of an INSTI.[22] This approach was used to predict the activities of XZ-259 against both WT and mutant INs. Figure 5D shows a comparison of the experimental IC$_{50}$ values with those predicted for each conformation. For the WT enzyme, conformation B was predicted to be more active than conformation A. However, both conformations predicted modest (2- to 8-fold) increases in IC$_{50}$ against the Y143R and N155H mutants and a greater increase (15- to 225-fold) against the G140S-Q148H mutant. These results match the observed fold changes of 2.6 (Y143R), 3.9 (N155H), and 57 (G140S-Q148H) in the biochemical assays. We cannot rule out that both conformations exist in the HIV-1 intasome or that mutations can shift the equilibrium between the two conformations.

Molecular Dynamics Applied to the HIV-1 Intasome to Explain Compound Activity. To date, there are cocrystal structures of the PFV intasome and almost a dozen compounds. However, those structures have not highlighted any specific property to explain the differences in the activity or resistance profiles of the drugs. Here, we have produced a series of related molecules with small structural differences that have a significant impact on their activity, and we used several molecular dynamics approaches to try to explain those differences.

Solvation was mapped in the HIV-1 IN model for the five XZ compounds, RAL and DTG (Figure 6). Displacing water molecules from direct interactions with the magnesium ions upon drug binding contributed unfavorably to the overall $\Delta G_{binding}$, as indicated by the red surfaces. The addition of a carbonyl group in XZ-89 and XZ-115 adds favorable solvation energy compared to XZ-90 and XZ-116 (Figure 6). This correlates with the small but reproducible beneficial effect observed on the ST inhibition potency in biochemical assays (Table 1). Similarly, the arrangement of halogens in XZ-89 and XZ-90 is more energetically favorable than the arrangement in XZ-115 and XZ-116. Again, this correlates with the 2-fold difference in IC$_{50}$ value observed *in vitro* (Table 1). The sulfone oxygens of XZ-259 contribute favorably in either conformation. Additionally, while the region around the S–N bond contributes favorably to the solvation energy of conformation A, the dimethylamine contributes favorably to the solvation energy of conformation B (Figure 6). By comparison, much of the favorable solvation for RAL binding involves the halobenzyl moiety, with an additional contribution from the oxadiazole moiety. A similarly large effect is seen for the halobenzyl moiety of DTG, and the effect is enhanced by the carbonyl group

linking it to the metal-binding core of the compound. Additional favorable contributions to DTG binding come from the ring oxygen of the oxazine ring and the exocyclic methyl group. Overall, it appears that the XZ compounds do not bind optimally in the hydrophobic pocket but that the highly favorable interaction of the sulfonamide group of XZ-259 is able to compensate for that suboptimal binding.

In the PFV intasome structures, the displaced terminal base (A$_{-1}$) can adopt two conformations that were incorporated into the HIV-1 models (Figure 6). The base appears to interact with the halobenzyl group of XZ-89, XZ-90, XZ-115, and XZ-116; however, it appears to interact with the chelating core of XZ-259. Because the HIV-1 model is based on the PFV structures where the displaced base is disordered, we calculated the $\Delta E_{binding}$ for the viral DNA end (including the last two nucleotides C$_{-2}$ and A$_{-1}$) upon binding of the five XZ compounds as well as RAL and DTG (Figure 7).
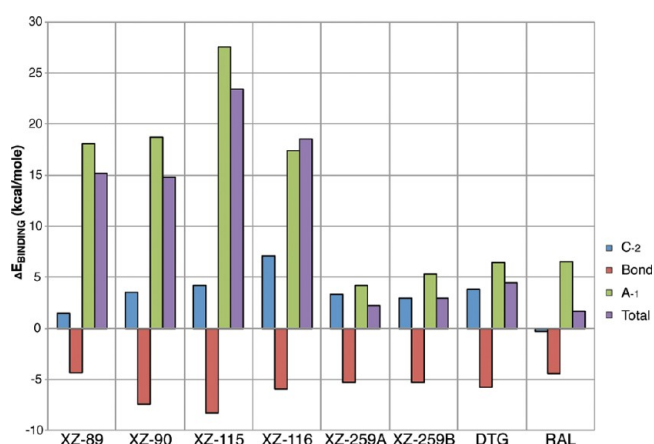

Figure 7. Binding energy profile of the viral DNA end. ΔE were calculated from the HIV-1 model upon binding of different INSTIs as indicated. C$_{-2}$ and A$_{-1}$ correspond to the two last bases of the viral DNA after processing and Bond corresponds to the phosphodiester between C$_{-2}$ and A$_{-1}$. Each $\Delta E_{binding}$ (C$_{-2}$, bond, and A$_{-1}$) is the sum of the $\Delta E_{internal}$ and $\Delta E_{interaction}$, while total is the sum of each $\Delta E_{binding}$ for C$_{-2}$, bond, and A$_{-1}$.

Looking at the $\Delta E_{binding}$ for C$_{-2}$, no obvious difference was observed among all the compounds, except for RAL, which had a negative $\Delta E_{binding}$ (Figure 7). This correlates with the fact that RAL's halobenzyl ring is more closely aligned to C$_{-2}$ than any of the other drugs, probably resulting in a better stacking of the base. However, a trend seems to exist for the four early XZ compounds. The C$_{-2}$ $\Delta E_{binding}$ tends to be higher when the chlorine is in *ortho* position as compared to *meta*. Moreover, having a carbonyl on the isoindoline ring system seems to lower $\Delta E_{binding}$ for C$_{-2}$, which correlates with the solvation effect observed previously (Figure 6). However, the $\Delta E_{binding}$ of the phosphodiester bond between C$_{-2}$ and A$_{-1}$ (bond) is similarly negative for all the drugs (Figure 7). This may result from relaxing strain on the backbone associated with base stacking.

It is in the A$_{-1}$ binding energy that the difference between compounds is the most striking. Two clusters are formed with XZ-89, XZ-90, XZ-115, and XZ-116 in one group and XZ-259, RAL, and DTG in the other. The first set of compounds present a highly positive $\Delta E_{binding}$ for A$_{-1}$ (between +17 and +27 kcal/mol), while the second set has a much smaller positive $\Delta E_{binding}$ (+4 to +6 kcal/mol). This correlates with the overall potency of the drugs. Despite the fact that XZ-259 is

structurally very similar to the other four XZ compounds, the dimethyl sulfonamide group is able to engage VdW interactions with both the sugar and the base of A_{-1}. Unfortunately, none of these properties appears sufficient to markedly affect the resistance profile. The determinants needed for the development of compounds that can evade the common resistance mutations still need to be defined. Nonetheless, making modifications to INSTIs to specifically enhance their interaction with the A_{-1} nucleoside seems beneficial in terms of their potency.

CONCLUSIONS

Starting from a series of dihydro-1*H*-isoindoline derivatives (XZ-89, XZ-90, XZ-115, and XZ-116), we developed a novel derivative, XZ-259. Herein, we report its activity and molecular pharmacology and compare its binding to the PFV and HIV intasomes with other known structures. While issues relative to the cytotoxicity of the series may be dependent on the integrity of the catechol function, insights from the cocrystal structures and molecular analyses suggest further modifications to improve the activity of the series. We propose that stabilization of the displaced adenosine (A_{-1}) is important for inhibitory potency.

METHODS

Small Molecules. XZ-89, XZ-90, XZ-115, and XZ-116 were synthesized according to previous protocols.[18,19] Preparation of XZ-259 was accomplished by a modification of these procedures and is reported in Supporting Information.

Oligonucleotides. Oligonucleotides were purchased from IDT (Integrated DNA Technologies Inc.). 5′-End radiolabeling of 21t (GTGTGGAAAATCTCTAGCAGT) and 19t (GTGTGGAAA-ATCTCTAGCA) was performed using T4 polynucleotide kinase (New England Biolabs), and unincorporated [γ-^{32}P]-ATP (Perkin-Elmer Life and Analytical Sciences) was removed by centrifugation using Mini Quick Spin oligo columns (Roche Applied Sciences), according to manufacturers' instructions. The 3′-P and ST substrates were generated by annealing an equimolar ratio of 21b (ACTGCTA-GAGATTTTCCACAC) to 21t and 19t, respectively.

IN Enzymes. Recombinant enzymes were expressed in *E. coli* from the pET15b-IN vector (producing a N-terminal 6-His tagged protein) and purified on nickel chelating column as described.[11] IN mutants were generated using the Stratagene QuikChange Site-Directed Mutagenesis Kit, according to the manufacturer's recommendations. The presence of desired mutations and the integrity of the remainder of the IN sequence were verified by DNA sequencing.

Integrase Reactions. IN reactions were carried out as previously described.[11] Briefly, drugs or an equivalent volume of 100% DMSO (dimethyl sulfoxide, used as the drug solvent) was added to a reaction mixture containing 20 nM ^{32}P-labeled DNA substrate and 400 nM IN in 50 mM MOPS pH 7.2, 7.5 mM MgCl$_2$, and 14 mM 2-mercaptoethanol. Reactions were performed at 37 °C for 1 h and stopped by the addition of an equal volume of loading buffer [formamide containing 1% SDS (sodium dodecyl sulfate), 0.25% bromophenol blue, and xylene cyanol]. Products were separated in 16% polyacrylamide denaturing sequencing gels. Dried gels were visualized using a Typhoon 8600 (GE Healthcare). Densitometric analyses were performed using the ImageQuant 5.1 software from GE Healthcare. Data analyses (linear regression, IC$_{50}$ determination, and standard deviation) were performed using Prism 5.0c software from GraphPad.

Antiviral Assays and Mutant Viruses. VSV-G pseudotyped HIV particles were obtained by cotransfection of 293 cells with pNLNgo-MIVR$^-$ΔEnv.LUC (derived from pNL4-3 by disruption of *env* and modified to express luciferase) and pCMV-VSV-G (encoding for the VSV-G glycoprotein) and used to infect HOS cells as previously described.[14] Mutant viruses were produced by site-directed mutagenesis of pNLNgoMIVR$^-$ΔEnv.LUC.

Cytotoxicity Assay. The 50% cytotoxicity concentrations (CC$_{50}$) were determined as previously described.[21] HOS cells were seeded in a 96-well luminescence cell culture plate at a density of 4000 cells in 100 μL per well. After 24 h, serial dilution of compounds is added to the culture medium, and plates are incubated at 37 °C for 48 h. Cytotoxicity was determined using ATPlite (PerkinElmer) according to the manufacturer's instruction. Data analysis and linear regression was performed using KaleidaGraph (Synergy Software).

Cocrystallization and Structure Determination. PFV intasome assembled with a double stranded DNA oligonucleotide mimicking the preprocessed U5 viral DNA end was crystallized, and the crystals were soaked with compounds as previously described.[16] X-ray diffraction data were collected at Diamond Light Source (Oxfordshire, UK) beamlines I02 (XZ-89 and XZ-259) and I03 (XZ-116), and at Swiss Light Source (Villigen PSI, Switzerland) beamline X06DA (XZ-90 and XZ-115). Structure refinement was performed starting from Protein Data Bank ID 3OYA. Data collection and refinement statistics are summarized in Supplementary Table 1.

Molecular Modeling. The HIV-1 intasome model used in this study was described in ref 22. Solvation analyses were performed using MOE2011.10 (Chemical Computing Group, Montreal, Quebec, Canada), as were the calculations of the DNA binding energies. This package includes the PFROSST force field, which treats proteins and nucleic acids with AMBER parameters and small molecules with parm@Frosst parameters. The PFROSST force field and Born solvation were applied to the energy minimizations and solvent calculations for all compounds. Coordinates of the compound and terminal adenosine from each of the PFV IN cocrystal structures were transferred directly into our model. Water molecules in direct contact with the metal ions were kept explicit, and all other water molecules were deleted. Complexes for each compound were energy minimized to an RMS gradient of 0.1. Solvation effects of drug binding were probed using MOE's Solvent Analysis tool. DNA binding energy calculations were done using the previously described MD approach with these updated force field and solvation parameters. Bond energies represent the difference between the calculated binding energies of the CA dinucleotide and the sum of the individual dC and dA energies for each complex. The *in vitro* activity predictions were performed using MOE2009.10 as previously described.[22]

Accession Codes. Coordinates and associated structure factors of solved structures for XZ-89, XZ-90, XZ115, XZ-116, and XZ-259 bound to the WT PFV intasome have been deposited with the protein data bank with ID codes 4bdy, 4bdz, 4be0, 4be1, and 4be2, respectively.

ASSOCIATED CONTENT

Ⓢ Supporting Information

Data collection and refinement statistics; preparation and synthesis of XZ-259. This material is available free of charge *via* the Internet at http://pubs.acs.org.

AUTHOR INFORMATION

Corresponding Author

* Tel: +1 (301) 496-5944. Fax: +1 (301) 402-0752. E-mail: pommier@nih.gov.

Author Contributions

$^\perp$These authors contributed equally to this work.

Notes

The authors declare no competing financial interest.

ACKNOWLEDGMENTS

■ REFERENCES

(1) Pommier, Y., Johnson, A. A., and Marchand, C. (2005) Integrase inhibitors to treat HIV/AIDS. *Nat. Rev. Drug Discovery 4*, 236−248.

(2) Li, X., Krishnan, L., Cherepanov, P., and Engelman, A. (2011) Structural biology of retroviral DNA integration. *Virology 411*, 194−205.

(3) Marchand, C., Maddali, K., Metifiot, M., and Pommier, Y. (2009) HIV-1 IN inhibitors: 2010 update and perspectives. *Curr. Top. Med. Chem. 9*, 1016−1037.

(4) Summa, V., Petrocchi, A., Bonelli, F., Crescenzi, B., Donghi, M., Ferrara, M., Fiore, F., Gardelli, C., Gonzalez Paz, O., Hazuda, D. J., Jones, P., Kinzel, O., Laufer, R., Monteagudo, E., Muraglia, E., Nizi, E., Orvieto, F., Pace, P., Pescatore, G., Scarpelli, R., Stillmock, K., Witmer, M. V., and Rowley, M. (2008) Discovery of raltegravir, a potent, selective orally bioavailable HIV-integrase inhibitor for the treatment of HIV-AIDS infection. *J. Med. Chem. 51*, 5843−5855.

(5) Pommier, Y., and Marchand, C. (2012) Interfacial inhibitors: targeting macromolecular complexes. *Nat. Rev. Drug Discovery 11*, 25−36.

(6) Hare, S., Gupta, S. S., Valkov, E., Engelman, A., and Cherepanov, P. (2010) Retroviral intasome assembly and inhibition of DNA strand transfer. *Nature 464*, 232−236.

(7) Marinello, J., Marchand, C., Mott, B. T., Bain, A., Thomas, C. J., and Pommier, Y. (2008) Comparison of raltegravir and elvitegravir on HIV-1 integrase catalytic reactions and on a series of drug-resistant integrase mutants. *Biochemistry 47*, 9345−9354.

(8) Metifiot, M., Marchand, C., Maddali, K., and Pommier, Y. (2010) Resistance to integrase inhibitors. *Viruses 2*, 1347−1366.

(9) Cooper, D. A., Steigbigel, R. T., Gatell, J. M., Rockstroh, J. K., Katlama, C., Yeni, P., Lazzarin, A., Clotet, B., Kumar, P. N., Eron, J. E., Schechter, M., Markowitz, M., Loutfy, M. R., Lennox, J. L., Zhao, J., Chen, J., Ryan, D. M., Rhodes, R. R., Killar, J. A., Gilde, L. R., Strohmaier, K. M., Meibohm, A. R., Miller, M. D., Hazuda, D. J., Nessly, M. L., DiNubile, M. J., Isaacs, R. D., Teppler, H., and Nguyen, B. Y. (2008) Subgroup and resistance analyses of raltegravir for resistant HIV-1 infection. *N. Engl. J. Med. 359*, 355−365.

(10) Fransen, S., Gupta, S., Danovich, R., Hazuda, D., Miller, M., Witmer, M., Petropoulos, C. J., and Huang, W. (2009) Loss of raltegravir susceptibility by human immunodeficiency virus type 1 is conferred via multiple nonoverlapping genetic pathways. *J. Virol. 83*, 11440−11446.

(11) Metifiot, M., Maddali, K., Naumova, A., Zhang, X., Marchand, C., and Pommier, Y. (2010) Biochemical and pharmacological analyses of HIV-1 integrase flexible loop mutants resistant to raltegravir. *Biochemistry 49*, 3715−3722.

(12) Metifiot, M., Vandegraaff, N., Maddali, K., Naumova, A., Zhang, X., Rhodes, D., Marchand, C., and Pommier, Y. (2011) Elvitegravir overcomes resistance to raltegravir induced by integrase mutation Y143. *AIDS 25*, 1175−1178.

(13) Hare, S., Smith, S. J., Metifiot, M., Jaxa-Chamiec, A., Pommier, Y., Hughes, S. H., and Cherepanov, P. (2011) Structural and functional analyses of the second-generation integrase strand transfer inhibitor dolutegravir (S/GSK1349572). *Mol. Pharmacol. 80*, 565−572.

(14) Metifiot, M., Johnson, B., Smith, S., Zhao, X. Z., Marchand, C., Burke, T., Hughes, S., and Pommier, Y. (2011) MK-0536 Inhibits HIV-1 integrases resistant to raltegravir. *Antimicrob. Agents Chemother. 55*, 5127−5133.

(15) Maertens, G. N., Hare, S., and Cherepanov, P. (2010) The mechanism of retroviral integration from X-ray structures of its key intermediates. *Nature 468*, 326−329.

(16) Hare, S., Vos, A. M., Clayton, R. F., Thuring, J. W., Cummings, M. D., and Cherepanov, P. (2010) Molecular mechanisms of retroviral integrase inhibition and the evolution of viral resistance. *Proc. Natl. Acad. Sci. U.S.A. 107*, 20057−20062.

(17) Langley, D. R., Samanta, H. K., Lin, Z., Walker, M. A., Krystal, M. R., and Dicker, I. B. (2008) The terminal (catalytic) adenosine of the HIV LTR controls the kinetics of binding and dissociation of HIV integrase strand transfer inhibitors. *Biochemistry 47*, 13481−13488.

(18) Zhao, X. Z., Semenova, E. A., Vu, B. C., Maddali, K., Marchand, C., Hughes, S. H., Pommier, Y., and Burke, T. R., Jr. (2008) 2,3-Dihydro-6,7-dihydroxy-1*H*-isoindol-1-one-based HIV-1 integrase inhibitors. *J. Med. Chem. 51*, 251−259.

(19) Zhao, X. Z., Maddali, K., Vu, B. C., Marchand, C., Hughes, S. H., Pommier, Y., and Burke, T. R., Jr. (2009) Examination of halogen substituent effects on HIV-1 integrase inhibitors derived from 2,3-dihydro-6,7-dihydroxy-1*H*-isoindol-1-ones and 4,5-dihydroxy-1*H*-iso-indole-1,3(2*H*)-diones. *Bioorg. Med. Chem. Lett. 19*, 2714−2717.

(20) Engelman, A., and Cherepanov, P. (2012) The structural biology of HIV-1: mechanistic and therapeutic insights. *Nat. Rev. Microbiol. 10*, 279−290.

(21) Zhao, X. Z., Maddali, K., Metifiot, M., Smith, S. J., Vu, B. C., Marchand, C., Hughes, S. H., Pommier, Y., and Burke, T. R., Jr. (2011) Development of tricyclic hydroxy-1*H*-pyrrolopyridine-trione containing HIV-1 integrase inhibitors. *Bioorg. Med. Chem. Lett. 21*, 2986−2990.

(22) Johnson, B. C., Metifiot, M., Pommier, Y., and Hughes, S. H. (2012) Molecular dynamics approaches estimate the binding energy of HIV-1 integrase inhibitors and correlate with *in vitro* activity. *Antimicrob. Agents Chemother. 56*, 411−419.

(23) Krishnan, L., Li, X., Naraharisetty, H. L., Hare, S., Cherepanov, P., and Engelman, A. (2010) Structure-based modeling of the functional HIV-1 intasome and its inhibition. *Proc. Natl. Acad. Sci. U.S.A. 107*, 15910−15915.

(24) Hare, S., Maertens, G. N., and Cherepanov, P. (2012) 3′-Processing and strand transfer catalysed by retroviral integrase *in crystallo*. *EMBO J. 31*, 3020−3028.